A technique to measure spin dependent trapping events at the metal-oxide-semiconductor field-effect transistor interface: near zero field spin dependent charge pumping

M. A. Anders[1], P. M. Lenahan[2], N. J. Harmon[3], and M. E. Flatté[4]

[1]Alternative Computing Group, National Institute of Standards and Technology, Gaithersburg, MD 20899, USA

[2]Department of Engineering Science and Mechanics, The Pennsylvania State University, University Park, PA 16802, USA

[3]Department of Physics, University of Evansville, Evansville, IN 47722, USA

[4]Department of Physics and Astronomy, The University of Iowa, Iowa City, IA 52242, USA

Abstract

We discuss a new technique to measure spin dependent trapping events at the metal-oxide-semiconductor field-effect transistor (MOSFET) channel/gate dielectric interface. We call this technique near zero field spin dependent charge pumping (NZF SDCP). It is based on a powerful MOSFET interface trap characterization measurement called charge pumping and related to an electrically detected magnetic resonance (EDMR) technique called SDCP. NZF SDCP and EDMR SDCP measurements are made on 4H-SiC MOSFETs, and we find that the introduction of nitrogen to the MOSFET interface can have a profound impact on the NZF SDCP response, which suggests that NZF SDCP may be useful to get atomic scale information about MOSFET interfaces such as defect identification. We also find that the NZF SDCP amplitude appears to saturate as a function of charge pumping frequency in most cases, but not all. We make model calculations to explain this behavior. We also find that the NZF SDCP spectrum broadens with increasing charge pumping frequency, which may be an inherent NZF SDCP phenomena. We hypothesize that NZF SDCP may also allow for experimental exploration of some magnetoresistance theories regarding interaction times between charge carriers and traps.

Introduction

Since the discovery of giant magnetoresistance [1], [2], magnetic spintronic devices have become an integral part of computing. They are typically used in hard drive read heads [3] and show promise as magnetic random access memory [4]. The success of this technology has sparked the study of organic and inorganic semiconductor spintronic devices. These devices provide a novel approach to, among other things, quantum computing [5] and magnetic field sensing [6]. Their utility comes from magnetoresistive phenomena exemplified by organic magnetoresistance (OMAR) [7], [8], magnetoelectroluminescence (MEL) [9], near zero field spin dependent trap assisted tunneling [10], and zero field spin dependent recombination [6], [11]. Some of these techniques show promise for extracting atomic scale information about defects involved in these processes [10], [11]. While the exact physical mechanisms responsible

for these phenomena are debated, all of them involve manipulating inherent spin dependent phenomena using only (typically small) magnetic fields. These magnetoresistive phenomena are typically measured as a change in resistance of a device current or, in the case of MEL, electroluminescence. In this work, we discuss a novel spintronic technique called near zero field spin dependent charge pumping (NZF SDCP) which involves measurement of spin dependent events related to charge capture at the channel/gate dielectric interface of metal-oxide-semiconductor field-effect transistors (MOSFETs). We note that "near zero field" refers to the quasi-static magnetic field magnitude which is exposed to the MOSFET.

NZF SDCP detects spin dependent events via current produced by the charge pumping (CP) measurement [12]–[14]. CP is a powerful electrical measurement used to characterize channel/gate dielectric interface traps in MOSFETs. The CP process, in the most straightforward approach, involves application of a continuous trapezoidal waveform to the MOSFET gate in order to alternately invert and accumulate the interface. This effect fills and empties the traps at the interface region. The trapezoidal gate waveform has a high time (t_H), defined as the time at which the gate waveform is at the highest voltage level (V_H), a low time (t_L), defined as the time at which the gate waveform is at the lowest voltage level (V_L), a rise time (t_r), defined as the time of the ramp, or rising edge, from V_L to V_H, and a fall time (t_f), defined as the time of the ramp, or falling edge, from V_H to V_L. The waveform repeats at some frequency called the charge pumping frequency (f_{CP}). Figure 1 illustrates a schematic of the gate waveform and its characteristic times and voltages. For an n-MOSFET, V_L is chosen such that it accumulates the interface (less than flat bands voltage) and V_H is chosen so that it inverts the interface (greater than threshold voltage). For our case, the source and drain are grounded. To understand the CP process, we first consider the gate to be at V_L. The interface is in accumulation and interface traps fill with holes. The gate voltage then ramps from V_L to V_H. When V_H is equal to threshold voltage, the interface inverts and free electrons from the source and drain diffuse into the channel. Some of the free electrons fill the interface traps. During the ramp from V_H back to V_L, the excess free electrons are allowed to diffuse from the channel back to the source and drain. Note that during the rising and falling edges of the pulse, some and electrons will thermally emit from the interface traps, but for short t_r and t_f, the effect is small. Back at V_L, the interface is accumulated and holes from the body recombine with the trapped electrons at the interface. The repeating CP process results in a net change in current from interface trap recombination called the charge pumping current (I_{CP}). I_{CP} is typically measured at the body contact and is given by [12]–[14]:

$$I_{CP} = q f_{CP} A_{eff} \overline{D_{it}} \Delta E_{CP}, \tag{1}$$

where q is the electronic charge, f_{CP} is the frequency of the trapezoidal gate waveform, A_{eff} is the effective channel area (the area of the channel which is made to invert and accumulate), and $\overline{D_{it}}$ is the mean density of interface states within the measured band gap energy window (ΔE_{CP}). ΔE_{CP} is nearly symmetric about mid gap and can be estimated by [12]–[14]:

$$\Delta E_{CP} = 2k_B T \ln\left(n_i \overline{v_{th}} \sqrt{\sigma_n \sigma_p} \sqrt{t_r t_f} \frac{|V_{FB}^{CP} - V_{TH}^{CP}|}{\Delta V_G} \right). \tag{1a}$$

Here, k_B is Boltzmann's constant, T is the temperature, n_i is the intrinsic carrier concentration, $\overline{v_{th}}$ is the geometric average of the electron and hole thermal velocity, t_r and t_f are the rise and

fall times of the gate waveform edges, respectively, $\Delta V_G = V_H - V_L$ is the waveform amplitude, V_{TH}^{CP} and V_{FB}^{CP} are the charge pumping threshold and flat band voltages, respectively, and σ_n and σ_p are the electron and hole capture cross sections, respectively. To measure the NZF SDCP effect, a CP measurement is made on a MOSFET placed in a small magnetic field which is swept from (e.g. 0 mT to 1 mT) or through (e.g. -1 mT to 1 mT) zero mT. I_{CP} is measured as a function of the magnetic field.

As is the case for many magnetoresistive-like processes, the underlying physical mechanisms involved in NZF SDCP is not fully understood. However, we can gain a qualitative knowledge by considering the spin dependence of recombination in semiconductors. The spin dependence of recombination is attributed to the formation of intermediate (pre-recombination) singlet and triplet spin pair states between conduction band electrons and paramagnetic defects [15], [16]. (For our case, the defects involved can be throughout a great majority of the band gap, as calculated from ΔE_{CP} in Eq. 1(a)) The singlet state S_0 has spin angular momentum S = 0 with m_s = 0. The triplet states T_-, T_0, and T_+ have spin angular momentum S = 1 with m_s = -1, 0 and +1, respectively. When an intermediate pair forms, for example in an excited state, and is in a triplet configuration, they dissociate, and the intermediate pair is broken. If the pair is in a singlet configuration, they relax to the ground state: the electron becomes trapped. Recombination then takes place when a hole is captured (typically fast). Thus, altering the singlet to triplet ratio will alter the recombination rate. This process is called spin dependent recombination (SDR). The full picture gets more complicated when adding CP elements such as the gate waveform which only allows for recombination during certain times. However, we believe a general understanding of SDR is enough to qualitatively understand our SDCP results. The mechanism responsible for mixing singlet and triplet states in NZF SDCP is likely hyperfine interactions [6]. Hyperfine interactions are interactions between an electron and nearby magnetic nuclei. The host atoms in our SiC devices have magnetic isotopes. They are ^{29}Si which is 4.7% abundant with I = 1/2 and ^{13}C which is 1.1% abundant with I = 1/2. Other magnetic nuclei such as ^{14}N and ^{1}H are also present and will be discussed later. This state mixing changes the ratio of singlet to triplet pairings which, as mentioned previously, alters the recombination rate. To understand why this can occur, we consider the spin Hamiltonian for an intermediate spin pair in an external magnetic field. Here we assume negligible exchange interaction:

$$\mathcal{H} = \mathcal{H}_0 + \mathcal{H}_{S-T}, \tag{2}$$

where

$$\mathcal{H}_0 = \frac{1}{2}\mu_B(g_1 + g_2)(\boldsymbol{S}_1 + \boldsymbol{S}_2) \cdot \boldsymbol{B}, \tag{2a}$$

$$\mathcal{H}_{S-T} = \frac{1}{2}\mu_B(g_1 - g_2)(\boldsymbol{S}_1 - \boldsymbol{S}_2) \cdot \boldsymbol{B} + \left(\sum_{j=0}^{m} a_{1,j}\boldsymbol{I}_j \cdot \boldsymbol{S}_1 + \sum_{k=0}^{n} a_{2,k}\boldsymbol{I}_k \cdot \boldsymbol{S}_2\right). \tag{2b}$$

Here, $\boldsymbol{S}_1$ and $\boldsymbol{S}_2$ are the spins of the free electron and paramagnetic defect, g_1 and g_2 are their g values, $\boldsymbol{I}_1$ and $\boldsymbol{I}_2$ are the nuclear spins of their host atoms, a_1 and a_2 are their hyperfine parameters, and $\boldsymbol{B}$ is an external magnetic field. $\mathcal{H}_0$ leads to the Zeeman splitting of the three

triplet energy levels by $g\mu_B B$. $\mathcal{H}_{S-T}$ leads to the mixing of the singlet and triplet states via hyperfine fields. Due to the varied configurations and physical positions of one or more nearby magnetic nuclei, each electron in the intermediate pair experiences slightly different hyperfine fields. This slight difference causes the state mixing [6]. Simply stated, in the absence of a magnetic field, there is some steady state current due to the CP process. As the magnetic field is increased, the T_- and T_+ triplet energy levels are split away from the S_0 level via the Zeeman interaction. The splitting reduces the singlet and triplet mixing and thus the recombination current. For our case, the effect is typically small, so we utilize a frequency and phase sensitive detection technique called lock-in detection by amplitude modulating the external magnetic field. In addition to significantly increasing signal-to-noise, the lock-in detection transforms the expected absorption-like NZF SDCP response into an approximate derivative. Thus, our measurements detect the spin dependent change in I_{CP}.

NZF SDCP is closely related to spin dependent charge pumping (SDCP) [17], [18], an electrically detected magnetic resonance (EDMR) [15] technique derived from electron spin resonance (ESR) [19]. However, the physical mechanisms involved in EDMR SDCP are much better understood. EDMR SDCP also detects spin dependent changes in I_{CP} via magnetic field manipulation of singlet and triplet populations. However, it relies on electromagnetic (EM) radiation to induce ESR to alter those populations. ESR occurs, for the simple case of an electron in free space, when EM radiation with energy $E_{ph} = h\nu$ equal to that of the electron Zeeman energy splitting $E = g_e\mu_B B$ is exposed to an electron causing it to "flip" its spin state from m_s = +1/2 to m_s = -1/2 or vice versa. Here, h is Planck's constant, ν is the electromagnetic radiation frequency (called the resonance frequency), g_e is the free electron g factor (g_e= 2.0023193…), μ_B is the Bohr magneton, and B is the magnetic field. By "flipping" the spins, the singlet and triplet populations are altered and, as mentioned previously, the device current is altered. We will consider a more complex case given by the Hamiltonian described by Eqs. 2. In this case, the g and a parameters describe the defect's local environment. Spin-orbit coupling causes the g values to deviate from the free electron g_e, and the a parameters provide a measure of the electron-nuclear hyperfine interactions. Analysis of the EDMR spectra in terms of equations in the form of Eqs. 2 allows definitive identification of the physical and chemical nature of defects. In fact, hyperfine spectra can be considered a defect "fingerprint" because they often give definitive proof of defect identification. Experimentally, the NZF and EDMR measurements can be very similar; the sole difference being that EDMR utilizes a source of EM radiation, and NZF does not. In this work, we compare similar NZF and EDMR SDCP measurements in order to learn more about the NZF response. We utilize two categories of EDMR resonance frequencies: ultra-low frequency (ULF) and X band. ULF measurements utilize a resonance frequency in the range of a few hundred MHz and X band measurements utilize a resonance frequency of about 9.5 GHz. In order to improve readability by reducing redundant acronyms, we will refer to NZF SDCP, ULF EDMR SDCP, and X band EDMR SDCP as NZF SDCP, ULF SDCP, and X band SDCP, respectively. EDMR SDCP will refer to both ULF and X band SDCP measurements simultaneously.

To complement our experimental observations, we make simulation calculations via the stochastic Liouville equation:

$$\frac{d\rho}{dt} = -\frac{2\pi i}{h}[\rho, \mathcal{H}] - k_s\{P_s, \rho\} - k_D\rho, \quad (3)$$

where ρ is an array representing the multi-spin density matrix, $\mathcal{H}$ is the spin Hamiltonian, k_s is the rate at which the two spins combine to form a non-paramagnetic center as a singlet state, k_D is the rate at which the pair dissociates. For these simulations, the Hamiltonian used in Eq. 3 considers one of the spins interacting with a single spin $I = 1/2$ nucleus. NZF SDCP is directly related to the singlet probability (ρ_S), and we can use Eq. 3 to calculate this directly. In order to model the trap filling and emptying dynamics in which the spin pair evolves, we integrate the singlet probability out to the upper time limit of $1/f_{CP}$ instead of using the steady state solution. We also replace $\sqrt{\sigma_n \sigma_p}$ in Eq. 1(a) with $\sqrt{\sigma_n' \rho_S \sigma_p}$ where σ_n' and σ_p are the spin independent electron and hole capture cross sections, respectively. ρ_S modifies the electron capture cross section while the hole capture cross section is assumed to always be spin independent. The resulting equation is:

$$I_{CP} = 2qk_BTf_{CP}A_{eff}\overline{D_{it}}\ln\left(n_i\overline{v_{th}}\sqrt{\sigma_n'\rho_S\sigma_p}\sqrt{t_rt_f}\frac{|V_{FB}^{CP} - V_{TH}^{CP}|}{\Delta V_G}\right), \quad (4)$$

With Eq. 3 and Eq. 4, we calculate the NZF SDCP response.

Experimental Details

Our NZF and ULF SDCP measurements were made on a custom-built spectrometer consisting of an electromagnet with 6 nested Hemholtz coils, a Kepco BOP 100-4M power supply, a Lake Shore Cryotronics 450 temperature-compensated Gaussmeter and Hall probe, and a computer which provides lock-in detection, magnetic field control, and data acquisition. The gate waveform is applied with a Tabor Electronics WW2572A waveform generator. ULF SDCP utilized a Doty Scientific surface coil and resonance circuit ($\nu \approx 380$ MHz) driven by a Stanford Research Systems SG380 radiofrequency (RF) signal generator. Figure 2 illustrates the ULF EDMR spectrometer. X band ($\nu \approx 9.5$ GHz) SDCP measurements were made on a custom-built EDMR spectrometer consisting of a Lake Shore Cryotronics magnet and power supply, a Resonance Instruments X band microwave bridge, a high Q factor TE_{102} X-band cavity, a Lakeshore 475 Gaussmeter and Hall probe, and a computer which provides lock-in detection, magnetic field control, and data acquisition. For EDMR measurements, the RF was coupled to the device by placing it within the center of the surface coil loop, and the X-band microwaves were coupled by placing the device into the high Q factor TE_{102} microwave cavity. For all measurements, we utilize lock-in detection by amplitude modulating the quasi-static external magnetic field at audio frequency, thus we measure the approximate derivative of the NZF and EDMR responses. Data shown as an "integral" spectrum was numerically integrated from the measured "derivative" response. Accounting for the accuracy of the Gaussmeter (0.002 mT), the accuracy of the current preamplifier used to measure the EDMR current, the accuracy of DAQ used to measure the preamp output, and the signal-to-noise ratio (>100), our relative magnetic field measurements have an uncertainty of less than 0.03% and our current measurements have an uncertainty of less than 0.01%, unless otherwise noted. For the X band measurements, the uncertainty in g-value calculations are less than 0.0003. The absolute magnetic field was calibrated with a "weak pitch" spin standard.

Two types of planar n-channel 4H-SiC MOSFETs were studied. One had an as-grown oxide with area (L x W) 1 x 424 um^2 and the other received a post oxidation anneal in NO at 1175 °C for 2 hours and had a gate area of (L x W) 1 x 1000 um^2. Both were grown on p-type epilayers. The samples were made by different manufacturers, but the primary processing difference is the post-oxidation NO anneal. This anneal significantly improves device performance [20], passivates interface states [21]–[23], and introduces a large density, about 10^{14} cm^{-2} [20], [23], of N at the SiC/SiO_2 interface. Table I summarizes sample parameters and extracted mean defect density via electrical CP measurements. For all measurements, a gate waveform with a 50% duty cycle and a 100 ns t_r and t_f was utilized. All measurements were made at room temperature.

Table I. Summary of sample parameters and characteristics of the MOSFETs.

Name	**Type**	**Oxide Process**	**Doping [cm^{-3}] × 10^{16}**	**$\overline{D_{it}}$ * [cm^{-2} eV^{-1}] × 10^{12}**	**Mobility [cm^2/Vs]**
as-grown	n-channel	N_2O wet thermal	6.0	3.0	1
NO annealed	n-channel	N_2O wet thermal + 2 hr NO anneal 1175 C	7.0	0.43	19

*D_{it} measurements made via charge pumping measurements

Results and Discussion

Figures 3a and 3b are ULF and NZF SDCP measurements from the as-grown and NO annealed samples, respectively. For the spectra labeled “rf on,” EM radiation is introduced to induce resonance. The “rf on” spectra show three large responses. The responses at -13.7 mT and 13.7 mT are expected; they are the resonance responses. The strong response at near-zero magnetic fields, however, is not due to resonance. The RF radiation was then turned off. The resulting measurements are illustrated by the patterns labeled “rf off.” We find that the responses at -13.7 mT and 13.7 mT are not present (as expected), however, the large response near zero magnetic field is still observed: its presence is unaffected by the RF. This is the NZF SDCP response.

Figures 3a and 3b show that the NZF SDCP responses from the as-grown and NO annealed samples are drastically different. The NZF SDCP response from the NO annealed sample is much broader than that of the as-grown sample (Fig. 3c). This is also the case for the ULF SDCP spectra (Fig. 3d). The increased broadening observed in the ULF SDCP case is due to hyperfine interactions from interfacial N introduced by the post-oxidation NO anneal [18]. N has a 100 % abundant $I = 1$ nucleus and, as mentioned previously, is found in very high densities at the SiC/SiO_2 interface [20], [23]. The same behavior is found for the case of magnetoresistance in organic semiconductors: increased hyperfine coupling broadens the magnetoresistance response [24]. Thus, we hypothesize that the broadening of the NZF response of the NO annealed sample is due to hyperfine interactions with interfacial N. If true, the simple NZF SDCP technique shows promise for detecting atomic-scale processing changes at MOSFET interfaces.

We also find that the response from the NO annealed sample appears to consist of two overlapping patterns. One is a broad line, and the other is a narrow line in the center of the broad response (Fig. 3c, bottom panel). The coexistence of broad and narrow features has been observed in radical pair reactions and have also been attributed to hyperfine interactions [25]. Additionally, broad features develop when there are many nuclear spins interacting with the paramagnetic spin [26]. Our simulations can explain the narrow and broad lines observed in the NO annealed sample. Figure 4 shows a representative calculated line shape. We hypothesize that there are two operating hyperfine couplings at work in the NO annealed sample; one gives rise to the broad line and may result from an ensemble of ^{29}Si and ^{13}C nuclei interacting with the electron spin, and one due to ^{14}N gives rise to the narrow line. A more quantitative modeling of the SDCP requires the inclusion of multiple nuclear spins interacting at one or both electron sites [26] and will be the subject of future work.

One dominating feature of as-grown NZF spectrum is the side peaks on either side of the dominating center line located at about 1 mT and -1 mT (Fig. 3c, top panel). The NO annealed sample spectrum does not exhibit these side peaks (Fig. 3c, bottom panel). Comparing the NZF response with ULF and X band SDCP spectra from the as-grown sample shows that all three measurements yield qualitatively similar patterns (Fig. 5). All measurements show a dominating center line with two smaller side peaks. For the case of the EDMR SDCP measurements, the side peaks are likely due to a defect called the 10.4 Gauss doublet [27], a hydrogen complexed oxygen vacancy. This defect has previously been observed in SiC MOSFETs [28]–[30]. The two-line spectrum comes from superhyperfine interactions with ^{1}H which has nearly 100 % abundant I = 1/2 nucleus. The slight asymmetry of these side peaks with respect to the dominating center line in the ULF measurements is due to the Breit-Rabi shift [31], a phenomenon driven by hyperfine interactions. In a previous work by Cochrane *et al.*, they observe a similar doublet magnetoresistance and EDMR spectra, however, they utilize SDR rather than SDCP [6], [11]. They conclude that the side peak structure in both the magnetoresistance and EDMR is due to resolved hyperfine interactions by using experimentally measured EDMR hyperfine parameters to calculate the singlet and triplet energies for an electron pair coupled to a 100% abundant I = 1/2 nucleus. They found that singlet-triplet energy crossings corresponded exactly to the locations of the side peaks in the magnetoresistance measurements [6]. Thus, we believe that the very simple NZF SDCP approach may be able to identify defect structure via resolved hyperfine interactions. The analysis of hyperfine interactions is the most useful aspect of EDMR for the identification of defects, and gives NZF SDCP promise as a low-cost, simple tool for MOSFET interface defect identification. However, a much deeper physical understanding of the NZF SDCP response must be developed in order to realize this potential.

To gain some insight into the dynamics introduced by the CP waveform, we compare NZF and ULF SDCP measurements as a function of f_{CP} (Fig. 6). Measurements from the as-grown sample (Fig. 6a) show that the NZF and ULF SDCP have similar f_{CP} responses. They both increase, then appear to saturate with increasing f_{CP}. Measurements on the NO annealed sample (Fig. 6b) show that the broad NZF line and ULF SDCP responses follow a similar behavior. The amplitudes increase, saturate, then slightly decrease. Although the broad NZF SDCP line appears to saturate, the narrow line clearly does not. Instead, it increases nearly linearly with increasing f_{CP}. For the EDMR case, the saturation behavior is tentatively attributed to the reduction of time allowed for the RF radiation to induce ESR. Simply, the time that a free electron and paramagnetic defect can interact as an intermediate spin pair is limited, for an n-

channel MOSFET, by t_H. As f_{CP} increases, t_H decreases, and so does the time allowed for ESR. This cannot strictly be the case for the NZF response because there is no ESR. However, our NZF model shows that the spin pair interaction times play a role. We find that the saturation behavior is due to the limit imposed on the spin pair interaction time by integrating the singlet probability out to the upper time limit of $1/f_{CP}$. Figure 7 displays the peak-to-peak amplitude for a range of f_{CP} values. The broad feature increases and then eventually levels off in accordance with the observations in Fig. 6. The narrow features, for the same hyperfine constant of 0.2 mT, increases much more sharply but also does plateau. As mentioned previously, we believe there are two operating hyperfine couplings working to produce the observed pattern. The fact that the couplings are different allows the narrow feature to climb nearly linearly over the range of f_{CP} while a smaller hyperfine interaction would lead to plateauing at smaller f_{CP}. A more quantitative modeling of the SDCP requires the inclusion of multiple nuclear spins interacting at one or both electron sites [26] and will be the subject of future work.

We also find that the NZF SDCP line width increases with increasing f_{CP}. Fig. 8a illustrates NZF SDCP line width as a function of f_{CP} for the as-grown sample. It increases from 0.48 mT with f_{CP} = 100 kHz to 0.75 mT with f_{CP} = 2 MHz. However, as illustrated by Fig. 8b, the SDCP line width does not change: it is 0.34 mT for all f_{CP}. The NZF SDCP response line width of the NO annealed sample also increases with increasing f_{CP}. The line width increases from 0.17 mT with f_{CP} = 100 kHz to 0.40 mT with f_{CP} = 2 MHz: the line width more than doubles. Figure 9a illustrates the NZF SDCP narrow center line at various f_{CP}. The SDCP line width increases, although not as dramatically (Fig. 9b), from about 0.44 mT with f_{CP} = 100 kHz to 0.5 mT with f_{CP} = 2 MHz. The broadening may be due to the shortening of interaction times between the free charge carrier and the trap. As mentioned previously, as f_{CP} is increased, the interaction time decreases. The previously mentioned work of Harmon *et al.* [32] also predicts line broadening with decreasing interaction time, as we observe in our measurements. The same conclusion is borne out by our calculations mentioned earlier. For instance, the narrow feature disappears as f_{CP} increases for a = 0.2 mT, k_S = 0.01 1/ns, and k_T = 0.001 1/ns (not shown). This is in agreement with Fig. 9(a). If so, this technique may be a way to experimentally investigate the effects of electron/trap interaction times and may be able to expand on the theory of magnetoresistance in general.

Conclusion

NZF SDCP is a new approach to spin dependent current measurement which likely involves similar physics as near zero magnetic field "magnetoresistive" phenomena observed in organic and inorganic semiconductors and insulators. We show that the introduction of N into the SiC MOSFET interface significantly changes the NZF SDCP response. We also give strong evidence that, in some cases, resolved hyperfine interactions can have a strong effect on the NZF SDCP pattern. This means that NZF SDCP could be a simple, cheap way to identify defects in MOSFET structures, however, a much deeper understanding of the NZF SDCP response must be developed. We find that the NZF SDCP response amplitude versus f_{CP} can be similar to that of SDCP, suggesting that similar physics is involved. However, we also find that it can be very different. The f_{CP}-dependent line broadening may be an inherent NZF SDCP phenomenon. NZF SDCP may be able to experimentally explore some of the magnetoresistance theories involved in other effects such as OMAR. We find, through model calculation of the hyperfine interaction,

some experimental observations can be understood by the restricted interactions times inherent to the SDCP technique.

Acknowledgements

This paper describes objective technical results and analysis. Any subjective views or opinions that might be expressed in the paper do not necessarily represent the views of the U.S. Department of Commerce or the United States Government. Certain commercial equipment, instruments, or materials are identified in this paper to foster understanding. Such identification does not imply recommendation or endorsement by the National Institute of Standards and Technology or the United States Government, nor does it imply that the materials or equipment identified are necessarily the best available for the purpose. Work at Pennsylvania State University, the University of Iowa, and the University of Evansville has been supported in part by the Defense Threat Reduction Agency under award number HDTRA1-18-0012. Work at Pennsylvania State University has also been supported in part by the U.S. Army Research Laboratory. The data that support the findings of this study are available from the corresponding author upon reasonable request.

Data Availability Statement

The data that support the findings of this study are available from the corresponding author upon reasonable request.

References

[1] M. N. Baibich *et al.*, “Giant magnetoresistance of (001)Fe/(001)Cr magnetic superlattices,” *Phys. Rev. Lett.*, vol. 61, no. 21, pp. 2472–2475, 1988, doi: 10.1103/PhysRevLett.61.2472.

[2] G. Binasch, P. Grünberg, F. Saurenbach, and W. Zinn, “Enhanced magnetoresistance in layered magnetic structures with antiferromagnetic interlayer exchange,” *Phys. Rev. B*, vol. 39, no. 7, pp. 4828–4830, 1989, doi: 10.1103/PhysRevB.39.4828.

[3] B. Dieny *et al.*, “Magnetotransport properties of magnetically soft spin-valve structures (invited),” *Journal of Applied Physics*, vol. 69, no. 8. pp. 4774–4779, 1991, doi: 10.1063/1.348252.

[4] S. Tehrani, B. Engel, E. Chen, M. DeHerrera, M. Durlam, and J. M. Slaughter, “Recent developments in magnetic tunnel junction MRAM,” *Dig. Intermag Conf.*, vol. 36, no. 5, pp. 2752–2757, 2000, doi: 10.1109/intmag.2000.872059.

[5] D. D. Awschalom and M. E. Flatté, “Challenges for semiconductor spintronics,” *Nat. Phys.*, vol. 3, no. 3, pp. 153–159, 2007, doi: 10.1038/nphys551.

[6] C. J. Cochrane, J. Blacksberg, M. A. Anders, and P. M. Lenahan, “Vectorized magnetometer for space applications using electrical readout of atomic scale defects in silicon carbide,” *Sci. Rep.*, vol. 6, no. October 2016, pp. 1–13, 2016, doi: 10.1038/srep37077.

[7] J. Kalinowski, J. Szmytkowski, and W. Stampor, “Magnetic hyperfine modulation of charge photogeneration in solid films of Alq3,” *Chem. Phys. Lett.*, vol. 378, no. 3–4, pp. 380–387, 2003, doi: 10.1016/j.cplett.2003.07.010.

[8] T. L. Francis, O.¨Mermer, G. Veeraraghavan, and M. Wohlgenannt, “Large magnetoresistance at room temperature in semiconducting polymer sandwich devices,” *New J. Phys.*, vol. 6, pp. 1–8, 2004, doi: 10.1088/1367-2630/6/1/185.

[9] Y. Wang, K. Sahin-Tiras, N. J. Harmon, M. Wohlgenannt, and M. E. Flatté, “Immense magnetic response of exciplex light emission due to correlated spin-charge dynamics,” *Phys. Rev. X*, vol. 6, no. 1, pp. 1–12, 2016, doi: 10.1103/PhysRevX.6.011011.

[10] M. J. Mutch, P. M. Lenahan, and S. W. King, “Spin transport, magnetoresistance, and electrically detected magnetic resonance in amorphous hydrogenated silicon nitride,” *Appl. Phys. Lett.*, vol. 109, no. 6, pp. 1–6, 2016, doi: 10.1063/1.4960810.

[11] C. J. Cochrane and P. M. Lenahan, “Zero-field detection of spin dependent recombination with direct observation of electron nuclear hyperfine interactions in the absence of an oscillating electromagnetic field,” *J. Appl. Phys.*, vol. 112, no. 12, 2012, doi: 10.1063/1.4770472.

[12] J. S. Brugler and P. G. A. Jespers, “Charge pumping in MOS devices,” *IEEE Trans. Electron Devices*, vol. 16, no. 3, pp. 297–302, Mar. 1969, doi: 10.1109/T-ED.1969.16744.

[13] G. Groeseneken, H. E. Maes, N. Beltran, and R. F. De Keersmaecker, “A Reliable Approach to Charge-Pumping Measurements in MOS Transistors,” *IEEE Trans. Electron*

Devices, vol. 31, no. 1, pp. 42–53, 1984, doi: 10.1109/T-ED.1984.21472.

[14] P. Heremans, J. Witters, G. Groeseneken, and H. E. Maes, "Analysis of the Charge Pumping Technique and Its Application for the Evaluation of MOSFET Degradation," *IEEE Trans. Electron Devices*, vol. 36, no. 7, pp. 1318–1335, 1989, doi: 10.1109/16.30938.

[15] D. Kaplan, I. Solomon, and N. F. Mott, "Explanation of the Large Spin-Dependent Recombination Effect in Semiconductors.," *J Phys Lett*, vol. 39, no. 4, 1978.

[16] P. M. Lenahan and M. A. Jupina, "Spin dependent recombination at the silicon/silicon dioxide interface," *Colloids and Surfaces*, vol. 45, no. C, pp. 191–211, 1990, doi: 10.1016/0166-6622(90)80023-W.

[17] B. C. Bittel, P. M. Lenahan, J. T. Ryan, J. Fronheiser, and A. J. Lelis, "Spin dependent charge pumping in SiC metal-oxide-semiconductor field-effect-transistors," *Appl. Phys. Lett.*, vol. 99, no. 8, pp. 1–4, 2011, doi: 10.1063/1.3630024.

[18] M. A. Anders, P. M. Lenahan, and A. J. Lelis, "Multi-resonance frequency spin dependent charge pumping and spin dependent recombination - applied to the 4H-SiC/SiO 2 interface," *J. Appl. Phys.*, vol. 122, no. 23, p. 234503, Dec. 2017, doi: 10.1063/1.4996298.

[19] J. A. Weil and J. R. Bolton, *Electron Paramagnetic Resonance*. Hoboken, NJ, USA: John Wiley & Sons, Inc., 2006.

[20] G. Y. Chung *et al.*, "Improved inversion channel mobility for 4H-SiC MOSFETs following high temperature anneals in nitric oxide," *IEEE Electron Device Lett.*, vol. 22, no. 4, pp. 176–178, 2001, doi: 10.1109/55.915604.

[21] R. Kosugi, T. Umeda, and Y. Sakuma, "Fixed nitrogen atoms in the SiO2/SiC interface region and their direct relationship to interface trap density," *Appl. Phys. Lett.*, vol. 99, no. 18, pp. 2009–2012, 2011, doi: 10.1063/1.3659689.

[22] G. Y. Chung *et al.*, "Effect of nitric oxide annealing on the interface trap densities near the band edges in the 4H polytype of silicon carbide," *Appl. Phys. Lett.*, vol. 76, no. 13, pp. 1713–1715, 2000, doi: 10.1063/1.126167.

[23] J. Rozen, S. Dhar, M. E. Zvanut, J. R. Williams, and L. C. Feldman, "Density of interface states, electron traps, and hole traps as a function of the nitrogen density in SiO2 on SiC," *J. Appl. Phys.*, vol. 105, no. 12, 2009, doi: 10.1063/1.3131845.

[24] T. D. Nguyen *et al.*, "Isotope effect in spin response of π-conjugated polymer films and devices," *Nat. Mater.*, vol. 9, no. 4, pp. 345–352, 2010, doi: 10.1038/nmat2633.

[25] C. R. Timmel, F. Cintolesi, B. Brocklehurst, and P. J. Hore, "Model calculations of magnetic field effects on the recombination reactions of radicals with anisotropic hyperfine interactions," *Chemical Physics Letters*, vol. 334, no. 4–6. pp. 387–395, 2001, doi: 10.1016/S0009-2614(00)01436-6.

[26] N. J. Harmon, S. R. McMillan, P. M. Lenahan, and M. E. Flatte, "A theoretical approach for analyzing radiation effects in Si/SiO2 MOSFETs," *IEEE Trans. Nucl. Sci.*

[27] T.-E. Tsai and D. L. Griscom, "On the structures of hydrogen-associated defect centers in irradiated high-purity a-SiO2:OH," *J. Non. Cryst. Solids*, vol. 91, no. 2, pp. 170–179, May 1987, doi: 10.1016/S0022-3093(87)80300-9.

[28] C. J. Cochrane, P. M. Lenahan, and A. J. Lelis, "Electrically detected magnetic resonance studies of processing variations in 4H SiC based MOSFETs," *Mater. Sci. Forum*, vol. 600–603, pp. 719–722, 2009, doi: 10.1109/ISDRS.2007.4422483.

[29] C. J. Cochrane, P. M. Lenahan, and A. J. Lelis, "An electrically detected magnetic resonance study of performance limiting defects in SiC metal oxide semiconductor field effect transistors," *J. Appl. Phys.*, vol. 109, no. 1, 2011, doi: 10.1063/1.3530600.

[30] M. A. Anders, P. M. Lenahan, C. J. Cochrane, and A. J. Lelis, "Relationship between the 4H-SiC/SiO2 interface structure and electronic properties explored by electrically detected magnetic resonance," *IEEE Trans. Electron Devices*, vol. 62, no. 2, pp. 301–308, 2015, doi: 10.1109/TED.2014.2364722.

[31] G. Breit and I. I. Rabi, "Measurement of Nuclear Spin," *Phys. Rev.*, vol. 38, no. 11, pp. 2082–2083, Dec. 1931, doi: 10.1103/PhysRev.38.2082.2.

[32] N. J. Harmon and M. E. Flatté, "Semiclassical theory of magnetoresistance in positionally disordered organic semiconductors," *Phys. Rev. B - Condens. Matter Mater. Phys.*, vol. 85, no. 7, 2012, doi: 10.1103/PhysRevB.85.075204.

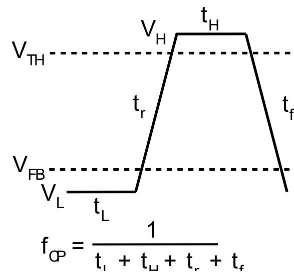

Figure 1. An illustration of the CP gate waveform and its parameters. V_L and V_H are the low and high gate waveform levels, t_L and t_H are the low and high gate waveform times, and t_r and t_f are the gate waveform rise and fall times, respectively.

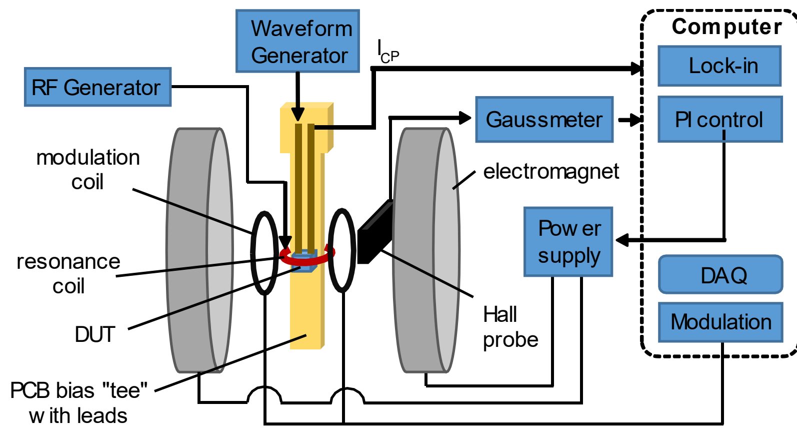

Figure 2. Schematic of the NZF and ULF SDCP measurement apparatus. The RF generator is on ULF SDCP measurements, and off for NZF SDCP measurements.

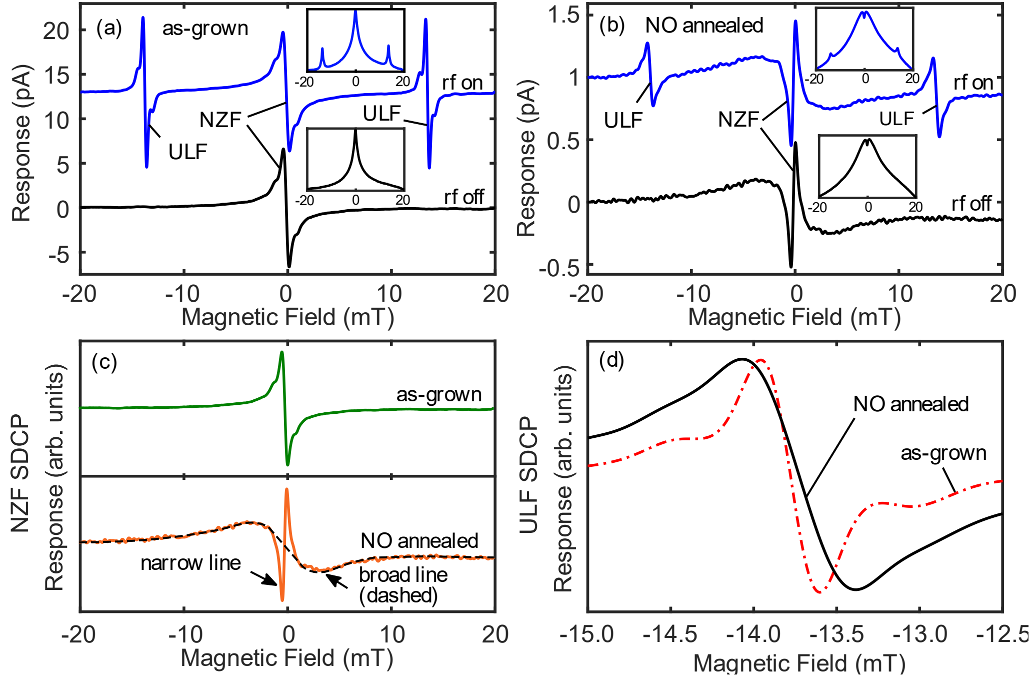

Figure 3. (a) ULF SDCP and NZF SDCP measurement on the as-grown and (b) NO annealed samples with and without RF radiation. (c) Is a comparison of the NZF responses from both samples. The dotted black line highlights the "broad" line. The "narrow" line is at the center. (d) Is a comparison of the ULF SDCP spectra from both samples. In all figures, the SDCP amplitudes are normalized to 1 for better comparison. The resonance frequency of the RF coil is 386 MHz and 383 MHz for as-grown and NO annealed measurements, respectively. The inset in (a) and (b) are the integrals of the ULF and NZF SDCP responses. For this measurement, V_H = 16 V, V_L = -16 V, and f_{CP} = 1 MHz. Modulation frequency and amplitude are 1 kHz and 0.15 mT, respectively.

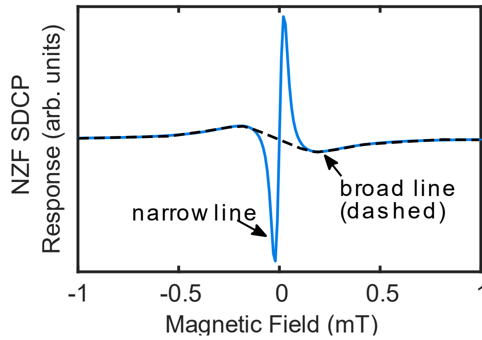

Figure 4. Calculation of NZF SDCP displaying the presence of both the broad and narrow features observed in the experiments. The inclusion of multiple spins by using a semiclassical approximation for the hyperfine interaction can further broaden the already broad line shape feature. Parameters: a = 0.2 mT, k_S = 0.01 ns^{-1}, k_T = 0.001 ns^{-1}, and f_{CP} = 0.5 MHz.

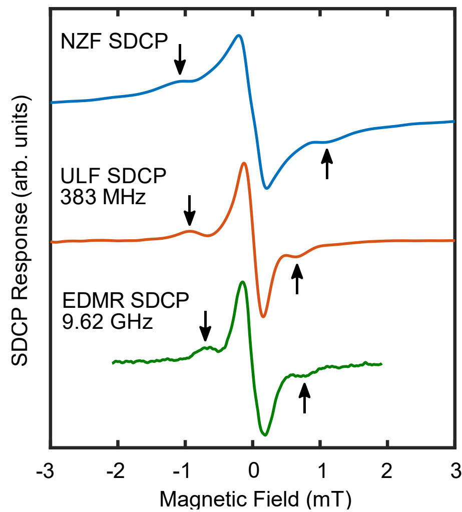

Figure 5. NZF, ULF (383 MHz), and X band SDCP (9.62 GHz) measurements from the as-grown sample. Traces are offset to 0 mT for better comparison. For this measurement, $V_H = 16$ V, $V_L = -16$ V, and $f_{CP} = 1$ MHz. Modulation frequency and amplitude are 1 kHz and 0.15 mT, respectively.

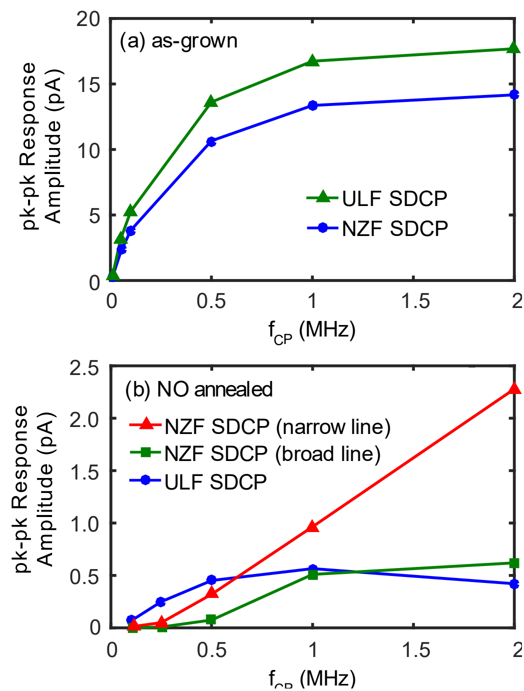

Figure 6. NZF and ULF SDCP peak-to-peak amplitudes for (a) the as-grown and (b) NO annealed samples. (b) Shows amplitudes for the two dominating lines shown in Fig. 3(c). Modulation frequency and amplitude are 1 kHz and 0.15 mT for the as-grown sample and 1 kHz and 0.25 mT for the NO annealed sample.

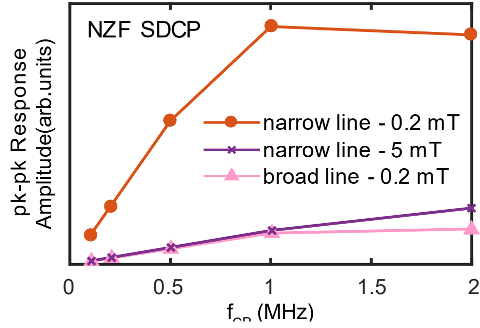

Figure 7. Relative peak-to-peak amplitudes for the narrow and broad features of NZF SDCP versus the charge pumping frequency. In the limit of high frequency, the amplitudes vanish (not shown). The plateauing observed for the lines with circle and triangle markers indicates the curves beginning to turn down. The timescale for amplitude to no longer increase with f_{CP} is determined by the hyperfine interaction and the spin-dependent rates k_S and k_T. Different hyperfine interactions can lead to different f_{CP} dependences as shown by the lines with circle and x markers.

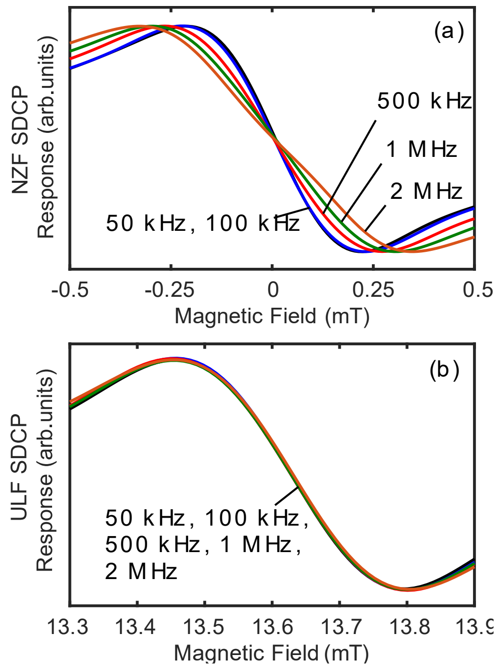

Figure 8. NZF and ULF SDCP measurements from the as-grown sample. (a) Illustrates the NZF SDCP line widths for f_{CP} = 50 kHz, 100 kHz, 500 kHz, 1 MHz, and 2 MHz, and (b) illustrates the ULF SDCP line widths for the same f_{CP}. For this measurement, V_H = 16 V and V_L = -16 V. The NZF SDCP line widths are 0.46, 0.48, 0.56, 0.65, and 0.73 mT for f_{CP} = 50 kHz, 100 kHz, 500 kHz, 1 MHz, and 2 MHz, respectively. The ULF SDCP line width is 0.34 mT for all f_{CP}. Response amplitudes are normalized for better comparison. Modulation frequency and amplitude are 1 kHz and 0.15 mT, respectively.

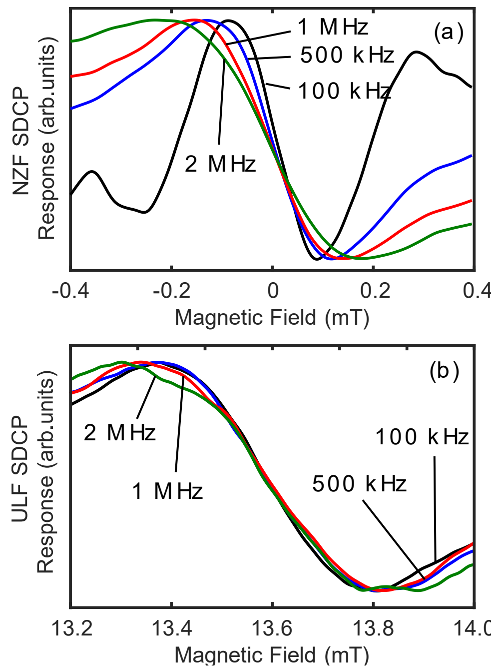

Figure 9. NZF and ULF SDCP measurements from the NO annealed sample. (a) Illustrates the NZF SDCP line widths for f_{CP} = 100 kHz, 500 kHz, 1 MHz, and 2MHz, and (b) illustrates the ULF SDCP line widths for the same f_{CP}. For this measurement, V_H = 5 V and V_L = -11 V. The NZF SDCP line widths are 0.17, 0.25, 0.30, and 0.40 mT for f_{CP} = 100 kHz, 500 kHz, 1 MHz, and 2 MHz, respectively. The ULRF SDCP line width is about 0.44, 0.44, 0.47, and 0.50 mT for f_{CP} = 100 kHz, 500 kHz, 1 MHz, and 2 MHz, respectively. Response amplitudes are normalized for better comparison. Modulation frequency and amplitude are 1 kHz and 0.15 mT, respectively.